ISBN: 978-3-95450-230-1 ISSN: 2673-5350 doi:10.18429/JACoW-IBIC2021-TUPP24

DEVELOPMENT OF A PROFILE MONITOR USING OTR AND FLUORESCENCE FOR INJECTED BEAMS IN J-PARC MAIN RING*

Y. Hashimoto†, Y. Sato, T. Toyama, T. Mitsuhashi, T. Nakamura, M. Tejima, M. Uota,
J-PARC Center, Tokai, Japan
also at Accelerator Laboratory, KEK, Tsukuba, Japan
H. Sakai[1], [1]Mitsubishi Electric System & Service Co., Ltd., Tsukuba, Japan

Abstract

A two-dimensional beam profile monitor having a high dynamic range approximately six digits of magnitude by using of Optical Transition Radiation (OTR) and fluorescence screens, Unit-1, has been operated in the injection-beam transport (3-50BT) line of the J-PARC main ring (MR) [1, 2]. This device contributes to the diagnosis of beam core and halo of intense proton beams before injection to MR, particularly measurement of beam cut effects by beam collimators located in upstream of the device is useful for beam shaping. We have been developing the second device, Unit-2, to be installed into MR for diagnosing on injected beams. By using the both of first and second devices, beam core and halo can be diagnosed in different phases. Property tests of the second device have been conducted at a test bench. But its longitudinal coupling impedance of several ohms (by *Z*/n value) is an issue. Then we have been studying the absorption of the rf power of the resonances up to about 1 GHz using SiC. In this paper, we discuss the characteristics of the developing device, and simulation results of reducing the coupling impedance.

INTRODUCTION

The key to increase beam intensity is how to reduce the beam loss, then the diagnosis of the beam halo with device of Unit-1 in operation has been an advantage. Following the Unit-1, it was planned to put a Unit-2 in MR [3, 4]. At the Unit-2, it will be able to diagnose a halo with a beam core and orbits of about 10 to 20 turns after the injection. Those two-dimensional information on the halo formation at the beginning of the circulation enables us to operate high-intensity beam with reflecting the correlation in the X-Y directions. In addition, by performing measurements synchronized with the Unit-1, it is possible to adjust the collimator balance between 3-50BT and MR, and to diagnose the transverse phase-space distribution of the injection beam including the two-dimensional XY coupling component. Furthermore, by only using the beam halo part of Unit-2 for the measurement of the circulating beam, the beam loss due to the time evolution of the two-dimensional distribution. It is also expected to diagnose resonance condition with such a temporal halo information.

Development as a basic monitor device has been completed, and basic measurements have been made on a test bench. The challenge for the current study is how to reduce the coupling impedance with MR circulating beams. At the beginning of development, the impedance (*Z*/n) was set to almost zero in the frequency range up to 100 MHz. This reason was the MR's basic acceleration frequency of 1.67-1.71 MHz (corresponding to 3-30 GeV) was observed with high-frequency components up to about 100 MHz in the actual beam. However, recently, microwave instabilities have occurred in the region of several hundred MHz at the time of rf de-bunch in a slow extraction. For this reason, a requirement was imposed to reduce the impedance in the region up to around 1 GHz to zero as much as possible.

DEVICE CONFIGURATION

The concept of a high dynamic-range profile monitor is to increase the dynamic range of detection by using two types of screens. The beam core (about 2 digits) is detected by OTR from the titanium screen, and the beam halo (about 4 digits) is detected by the fluorescence from the alumina screen on the outer part [1, 2] (Fig. 1).

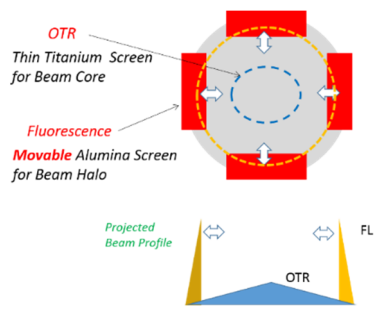

Figure 1: Conceptual screen layout.

In the Unit-2, the following five points were changed from the Unit-1 of 3-50 BT in order to install it in MR.

1. The diameter of the beam hole at the upper concave mirror was increased from 120 mm to 160.
2. Then the diameter of the concave mirror was increased from 300 mm to 350 mm to compensate for the light loss due to the large beam hole as above.
3. The vacuum chambers for the mirror and the target were separated.
4. The imaging point was positioned in the atmosphere to increase the yield of light with close optics.
5. Though conventional mirrors were made by depositing pure aluminium on the entire surface of polished Pyrex glass, considering radiation damage, in Unit-2 pure aluminium (A1050) was used as the base material and machined.

* Work supported by Grant-in-Aid for Scientific Research JP16H06288.
† email address: yoshinori.hashimoto@kek.jp

ISBN: 978-3-95450-230-1 ISSN: 2673-5350 doi:10.18429/JACoW-IBIC2021-TUPP24

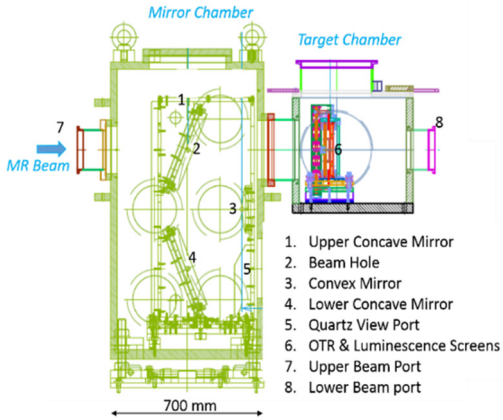

Figure 2: Layout of the device apparatus.

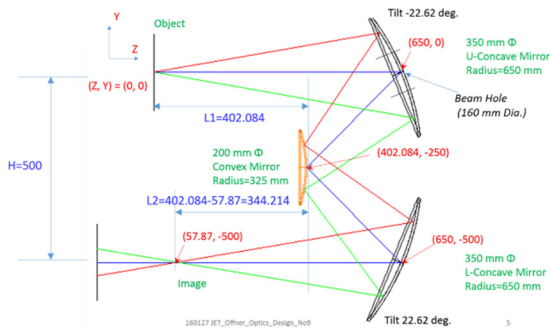

Figure 3: Layout of Offner relay optics.

Figures 2 and 3 show the configurations of the device and the relay optical system, respectively. The optical system transfers the OTR and fluorescence generated at the target to imaging point. The Offner optical system consisting of upper and lower concave mirrors with a diameter of 350 mm and convex mirrors with a diameter of 200 mm [5], and these three surfaces are concentric spheres. The system has a large aperture as that F value is about 0.7. The spread angle of the OTR by the 3 GeV injected proton beam is 27 degrees [1, 2], and the mirror is large enough to cover the solid angle. These spherical mirrors using aluminium (A1050) were made by lathe processing with an air bearing type lathe, then it was possible to achieve a surface accuracy of about 6 to 60 nm in terms of Ra (arithmetic mean roughness) value. The wave surface accuracy was about $\lambda/4$. The optical system was confirmed by a grid pattern test to have a horizontal field of view of 140 mm and a vertical field of view of 100 mm. For the difference in light transmittance depending on the location of the subject, a sensitivity map was created by sweeping the laser spot. It is used to correct the beam measurement data.

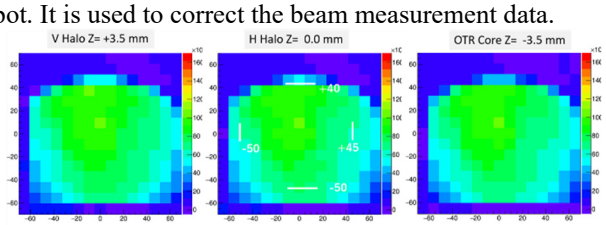

Figure 4: Transmission map by laser swept from 3 types of target positions.

Figure 4 shows uniform transmission area within un-uniformity 15% was 80 mm square. Target position varied ±3.5 mm which amount to actual target differences, the results show almost the same transmission map. They also show that the depth of field can be secured at 7 mm.

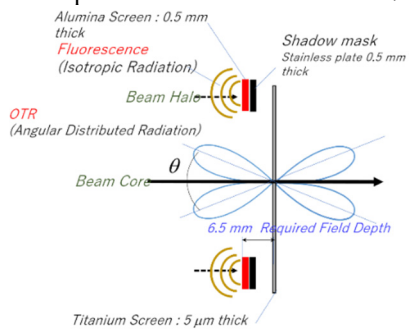

Figure 5: Target configuration.

A target configuration is shown in Fig. 5. A titanium foil screen for beam core with a thickness of 5 μm, and the red rectangles located on the top, bottom, left, and right of alumina screens for beam halo with a thickness of 0.5 mm. Table 1 summarizes the losses in these materials for high intensity beams.

Table 1: Energy Loss in the Screen Materials

	Energy Loss [keV/proton]**	Energy Loss [J/bunch]***
Titanium 5 μm	3.4	4.9e-3
Alumina 0.5 mm	330	4.7e-1

* 3GeV Proton, ** 1e13 proton/bunch

The durability of titanium foil is not a problem even when a high-intensity beam such as 7.6×10^{13} proton / 2bunch was circulated and passed through the foil for about 100 turns (repetition cycle 5.3 μs) at MR [6]. The total energy loss value of alumina in the table is about 100 times larger than that of titanium. However, since the proton density at the alumina target is 10^{-3} or less to the beam center because of beam halo part, the actual total energy loss during use is 1/10 or less of that of titanium, and no problem occurs. Concerning beam spread of these screen materials due to scattering were estimated to be about 1 %/10 turns for the titanium foil in the beam core and 50 %/10 turns for the alumina in the beam halo. Although the alumina screen for the beam halo has the above-mentioned scattering effect, it is also taken into consideration that the beam halo growth exceeding 40 π mm.mrad will be captured by measuring not only the injection time but also during acceleration.

The secondary optical system locates in a lead shield under the target where the radiation exposure dose was about 500-1000 mGy/week by pre-measured using the OSL chip [7] during operation of the high intensity beam. This dose level was almost the same as the value at the Unit-1. The components of the secondary optical system consist of a quartz diffuser plate at the imaging point to convert OTR into scattered light, and a close-range wide-angle optical

ISBN: 978-3-95450-230-1 ISSN: 2673-5350 doi:10.18429/JACoW-IBIC2021-TUPP24

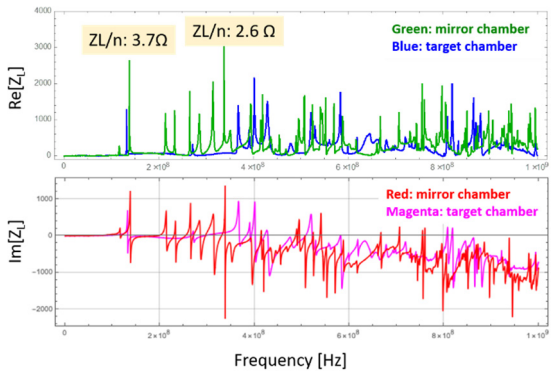

Figure 6: Results of coupling impedance measurement with initial equipment.

system for obtaining beam image. The basic measurement system is a wide dynamic-range CMOS camera with an image intensifier with rise time of 100 ns.

COUPLING IMPEDANCE

Impedance measurements [8] using wire were performed on each of the mirror chamber and the target chamber (Fig. 6). For the impedance value, Z/n [Ω] used for the evaluation of instability is used, when n = frequency/revolution frequency. In up to 1 GHz, the mirror chamber had a peak of 3.7 Ω around 150 MHz and a peak of 2.6 Ω near 350 MHz. In the higher frequency region, there were many peaks of about 1.5 Ω or less. In the target chamber, most of the peaks were below about 0.5 Ω.

The slow extraction beam has a high intensity of about 65 kW currently, and microwave instability occurs depending on conditions at the time of de-bunch at 30 GeV. According to the Keil-Schnell criterion [9, 10], which is often used as a measure of the onset of this instability, the MR threshold is estimated to be about several Ω. By a consideration, it was decided to reduce the impedance to about 0.5 Ω or less as much as possible. Therefore, the mirror chamber should be reduced these impedances.

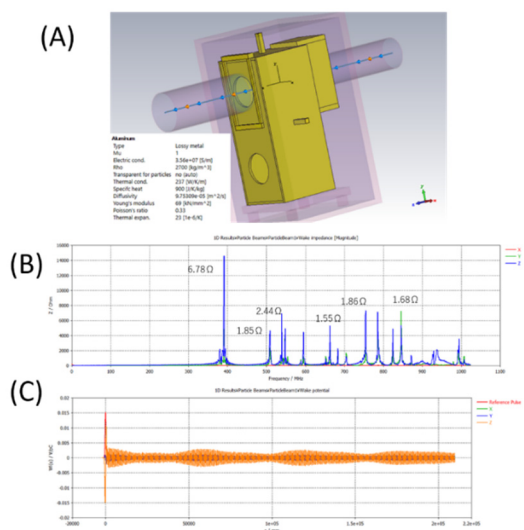

Figure 7: Simulation with a shielded Mirror Unit: (A) Structure, (B) Impedance, (C) Wake potential.

IMPEDANCE REDUCTION

By Structure Modifying

We conducted simulation by wake solver of CST Studio suite [11] to reduce various resonances. However, it is difficult to make Z/n sufficiently small, and particularly, the problem was the resonance does not decay by next bunch. For example, Fig. 7 shows an example of a simulation in which the internal mirror unit was covered by an aluminium shield. There was a high resonant peak of 6.78 Ω at 390 MHz, and some resonances remained at higher frequencies (Fig. 7 (B)). Figure 7 (C) shows the wake potential did not decay by the next bunch sufficiently. In Fig. 7, the impedance values(B) are just the lower limits in simulation because of not enough time region(C) to decay them.

Field Absorption Using Silicon Carbide

Therefore, we decided to study a method of absorbing an electric field using a dielectric. For the dielectric, silicon carbide (SiC) [12-14], which has been proven to be used for the purpose of attenuating higher-order modes in accelerating cavities such as KEKB and KEKB DR, was selected. SiC is CoorsTek's CERASIC B [15] (Fig. 8), especially suitable for the frequency above 100 MHz. The absorption power P of the high frequency electric field by the dielectric is given by Eq. (1). Here, with K as a constant, ε' is the relative permittivity, $\tan\delta$ is the dielectric loss angle, f is the frequency, and E is the electric field strength,

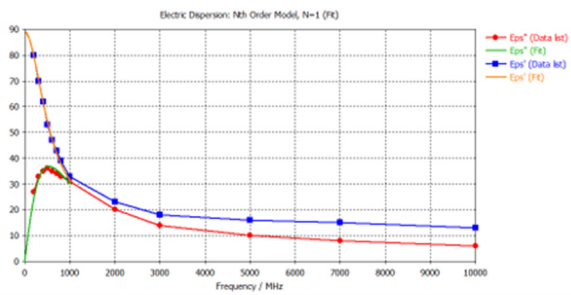

Figure 8: Permittivity of a SiC, ε': blue, and ε'': red.

$$P = K \cdot \varepsilon' \cdot tan\delta \cdot f \cdot E^2 \qquad (1).$$

Simulation with SiC

For the electric field absorption in SiC, it is effective to install it in a place where the normal electric field strength is larger (Eq. (1)). However, in order to remove heat generated by absorption, it is easier to install it at a position facing the atmosphere than inside a vacuum chamber. For this reason, we decided to install SiC on the vacuum side of the inner surface of the port flange of the mirror chamber.

The configuration in which SiC was attached to a total of 9 surfaces, 8 surfaces of the ICF253 flange on the side of the chamber and 1 surface of the ICF406 flange on the top surface. This set had a high effect on impedance

ISBN: 978-3-95450-230-1 ISSN: 2673-5350 doi:10.18429/JACoW-IBIC2021-TUPP24

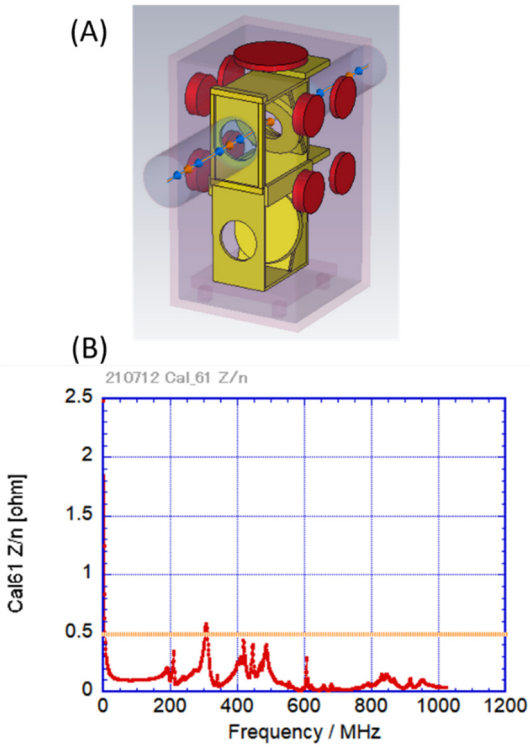

Figure 9: A wake field simulation with SiC, (A) red plates mean SiC, and (B) wake impedances.

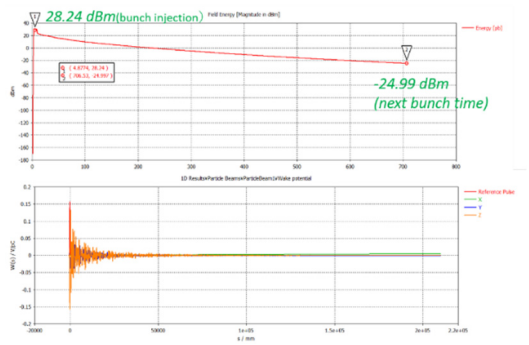

Figure 10: Calculated field energy (A) and wake potential (B) during one-bunch time separation of 700 ns.

reduction (Fig. 9(A)). The position of the SiC plate of ICF253 on the downstream side of the beam level was increased SiC thickness to 60 mm because the viewing space in the cavity was wide, and the others were 30 mm. The longitudinal impedance had the maximum peak of 0.6 Ω at 250 MHz, and the others were below the target of 0.5 Ω (Fig. 9 (B)). Figure 10 shows the varying with time in the field power and in wake potential of one bunch interval. The field is 28.24 dBm (0.66 W) when passing through the bunch and is attenuated gradually by 52 dB during the bunch time. This calculation assumes 3×10^{12} protons per bunch and that all power is absorbed by SiC. In a actual case, bunch of 5×10^{13} protons, it can be estimated to be about 11 W. In addition, the wake potential decays at about 1/3 of the bunch time interval.

SUMMARY AND PROSPECTS

We have been developing the second profile monitor using OTR and fluorescence in order to increase the intensity of J-PARC MR and to improve the diagnostic equipment for injected beams. The device was completed with the configuration as designed, and the characteristics have been measured on the test bench. For installation on MR, there was a requirement to reduce the coupling impedance with the beam to about 0.5 Ω or less and as small as possible in order to reduce beam instability. By adding SiC as a countermeasure, we obtained simulation results with an impedance of about 0.6 Ω. In the near future, SiC plates will be manufactured and impedance measurement will be performed on the bench.

ACKNOWLEDGEMENTS

We have received a lot of cooperation regarding SiC from KEK Yasunao Takeuchi.

REFERENCES

[1] Y. Hashimoto, T. Toyama, T. M. Mitsuhashi, M. Tejima, and S. Otsu, “A Development of High Sensitive Beam Profile Monitor using Multi-Screen”, in *Proc. 2nd Int. Beam Instrumentation Conf. (IBIC'13)*, Oxford, UK, Sep. 2013, paper TUCL2, pp. 338-341.

[2] Y. Hashimoto *et al.*, “Two-Dimensional and Wide Dynamic Range Profile Monitor Using OTR / Fluorescence Screens for Diagnosing Beam Halo of Intense Proton Beams”, in *Proc. 54th ICFA Advanced Beam Dynamics Workshop on High-Intensity and High-Brightness Hadron Beams (HB'14)*, East Lansing, MI, USA, Nov. 2014, paper TUO2AB04, pp. 187-191.

[3] Yoichi Sato *et al.*, in *Proc. of the 16th Annual Meeting of Particle Accelerator Society of Japan*, July 2019, Kyoto, Japan, pp. 1125-1129. (In Japanese), https://www.pasj.jp/web_publish/pasj2019/proceedings/PDF/FRPI/FRPI038.pdf

[4] S. Igarashi *et al.*, “Accelerator design for 1.3-MW beam power operation of the J-PARC Main Ring”, *Prog. Theor. Exp. Phys.*, vol. 2021, p. 033G01, 2021. doi:10.1093/ptep/ptab011

[5] A. Offner, “New concepts in projection mask alignment”, *Optical Engineering*, vol. 14, no. 2, p.130-132, 1975.

[6] Y. Hashimoto *et al.*, “Multi-Ribbon Profile Monitor Using Carbon Graphite Foil for J-PARC”, in *Proc. 46th ICFA Advanced Beam Dynamics Workshop on High-Intensity and High-Brightness Hadron Beams (HB'10)*, Morschach, Switzerland, Sep.-Oct. 2010, paper WEO2A01, pp. 429-433.

[7] T. Okazaki *et al.*, in Proc. 15th PASJ annual meeting, Nagaoka, 2018, pp1256-1259, https://www.pasj.jp/web_publish/pasj2018/proceedings/PDF/THP1/THP137.pdf

[8] T. Toyama, “Beam Instrument”, OHO 2009 (In Japanese), http://accwww2.kek.jp/oho/OHOtxt3.html

[9] K. Keil and W. Schnell, “Concerning longitudinal stability in the ISR”, CERN, Geneva, Switzerland, Rep. CERN-ISR-TH-RF/69-48, Jul. 1969.

[10] Y. H. Chin, “Beam instability on high intensity proton

ISBN: 978-3-95450-230-1 ISSN: 2673-5350 doi:10.18429/JACoW-IBIC2021-TUPP24

beam", OHO 2005 (In Japanese), http://accwww2.kek.jp/oho/OHOtxt3.htm

[11] CST Studio suite, https://www.3ds.com/ja/products-services/simulia/products/cst-studio-suite

[12] Y. Takeuchi, T. Abe, T. Kageyama, and H. Sakai, "RF Dielectric Properties of SiC Ceramics and their Application to Design of HOM Absorbers", in *Proc. 21st Particle Accelerator Conf. (PAC'05)*, Knoxville, TN, USA, May 2005, paper WPAT010, pp. 1195-1197.

[13] T. Kageyama, T. Abe, H. Sakai, and Y. Takeuchi, "HOM Damping of ARES Cavity System for SuperKEKB", in *Proc. 21st Particle Accelerator Conf. (PAC'05)*, Knoxville, TN, USA, May 2005, paper TPPT010, pp. 1186-1188.

[14] Y. Takeuchi, "Design for Microwave Circuit", OHO 2017 (In Japanese), http://accwww2.kek.jp/oho/OHOtxt4.html

[15] Coorstek, KK, CERASIC B, http://www.coorstek.co.jp/jpn/products/detail/detail_19.html